

Chapter 3

COMPARISONS OF EXPERIMENTAL AND FINITE ELEMENT ANALYSIS RESULTS

Before three dimensional numerical test of four connection systems in chapter 4, the author would like to compare the experiemental test results and numerical methods. The reasons for this comparison are to check the reliability of Finite Element's procedures for the interaction between the node connector and beam element and to implement numerical analysis of moment-rotation behavior taking geometric and material nonlinearities more appropriate simulating method into consideration.

For the implementation of the Finite Element Analysis(FEA), two node connection systems could be introduced, thanks to the data of real experiments performed by Lehmann & Keller Engineers GmbH, Germany(HEFI-1) and Schlaich Bergermann und Partner Structural Consulting Engineers, Germany(SBP-3). All the procedures, which have been performed in this chapter, will be a guidline for the numerical simulation for the next chapter.

3.1 Node connection system HEFI-1

3.1.1 Geometrical details of experiment

The splice node connection HEFI-1 has two flat disks with a circular groove and four holes (Figure 3.1). In 1993, the German company Helmut Fischer GmbH, Talheim, contracted for various loading tests of node connector HEFI-1 with Versuchsanstalt fuer Stahl, Holz und Steine (VA) of University Karlsruhe, Germany for the roof project in the hippopotami house of the zoological garden in Berlin (Figure 3.2).

The details of node connecting specimen used in the experiment are shown in Figure 3.4. This node connector is a star-shaped connecting, which consists of six beams with two flat disks. The end part of the beam was star-shaped so that it could be matched with the star-shaped angles of the other end of beam. And then they were jointed together and connected with one cylinder-head bolt M12. Each beam's length is 500 mm with a section of 40 mm×60 mm. And the thickness of the disc is 10 mm with 110 mm diameter. The deviation between bolt and hole was 0.1 mm. The center of connector is 4° higher from horizontal level which were vertically loaded with 4 kN/min (Figure 3.3~3.5).

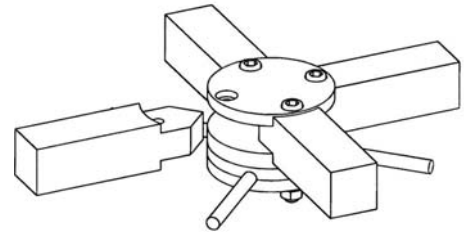


Figure 3.1:
Node connection system HEFI-1
[Stephan et al 2004]

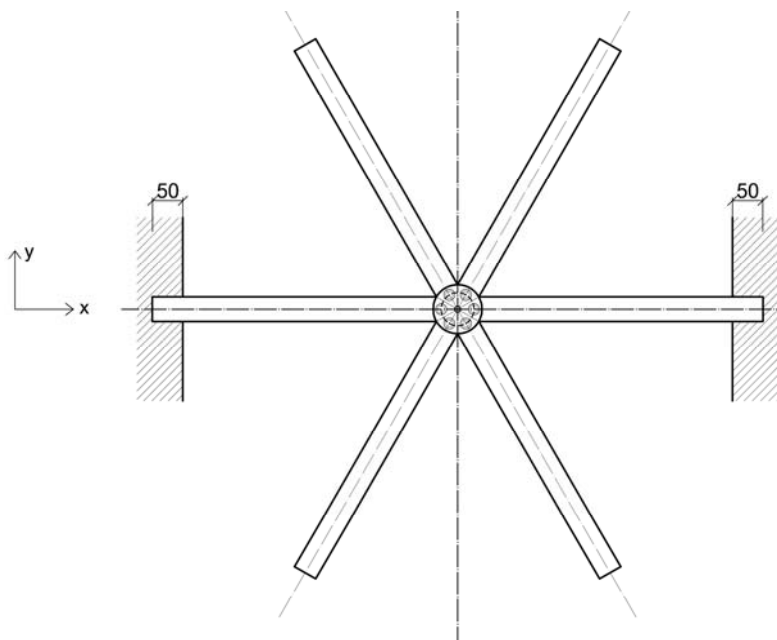


Figure 3.2:
The hippopotami house of the zoological garden in Berlin [Schlaich et al 2003]

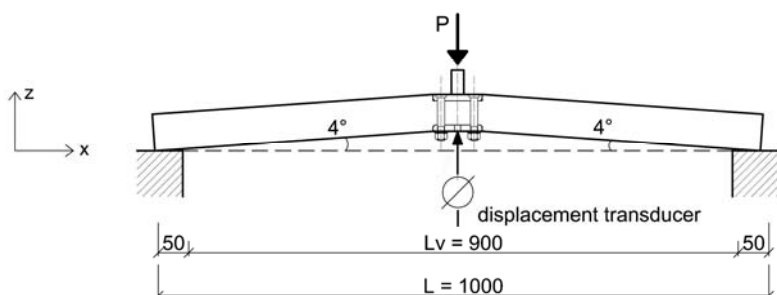


Figure 3.3: Test set-up of bending test (mm) [Fischer 1993]

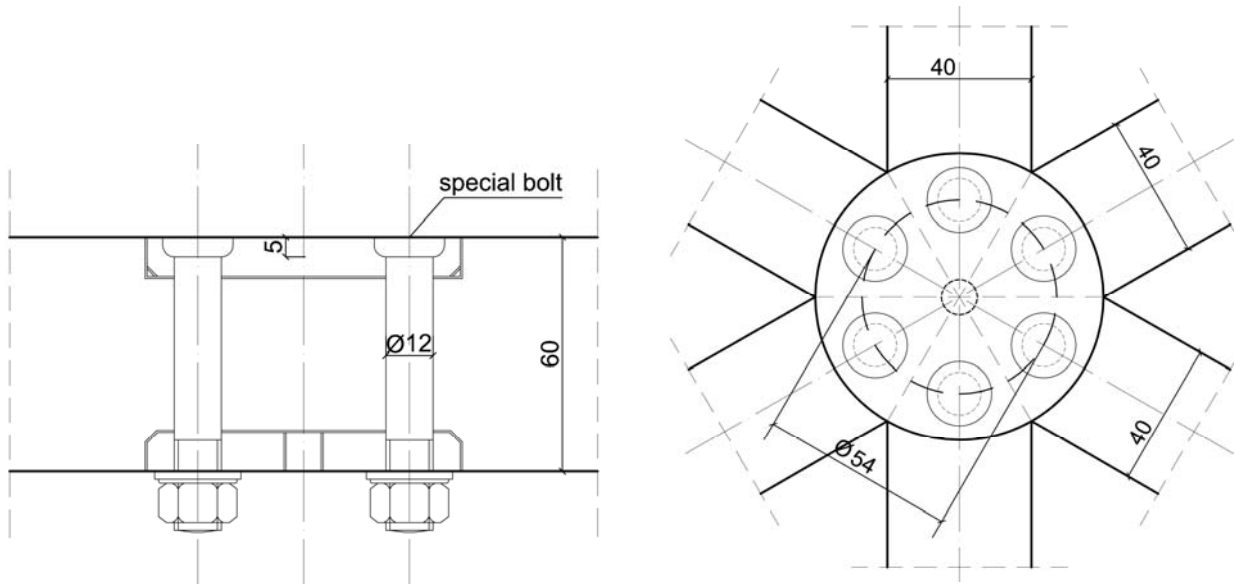


Figure 3.4: Connector's details of HEFI-1 (mm) [Fischer 1993]

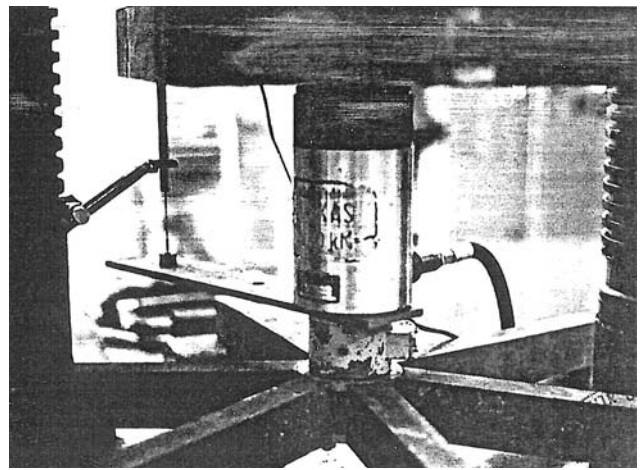
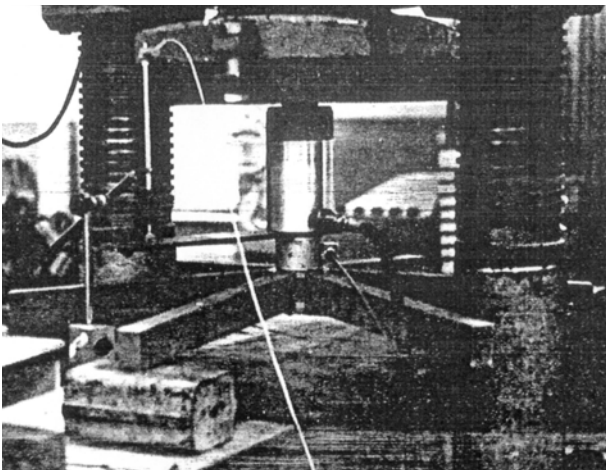


Figure 3.5: Experimental bending test of HEFI-1 [Fischer 1993]

3.1.2 Finite element model

In the Finite Element model, all elements of the beam, disc plates and bolt were meshed by the 10-node tetrahedral solid structural elements SOLID 92 which has a quadratic displacement behavior. This element is well suited to model irregular meshes, such as produced from various CAD/CAM systems [ANSYS v.11 2009], and all geometric models used for this simulation of HEFI-1 was from CAD package Rhino version 4.0.

In terms of contact modeling, the beam members and two disc plates are assumed to be assembled together by means of bolts. When load is applied to the structure, some parts of the surfaces separate while the remainder holds. If no stiffness exists, under the application of load, one surface will penetrate another. In order to simulate for the behaviour of such surfaces that may break contact interface elements are necessary. An interface element operates by attaching an imaginary spring element between nodes along the surface boundary. A stiffness is assigned to the spring element when two surfaces interpenetrate. When interpenetration is identified, equilibrium is implemented by [Harte et al 2001].

$$P = k \times \delta_i \quad (3.1)$$

P : the applied load

k : the spring stiffness

δ_i : the amount of the interpenetration

Some interpenetration of surfaces will always occur when the spring stiffness is not infinitely large. Very large spring stiffness may cause convergence difficulties, therefore ANSYS recommends a value of the spring stiffness equal to a factor f times the elastic modulus of the material [ANSYS v.11 2009] [Harte et al 2001].

$$k = f \times E \quad (3.2)$$

E : elastic modulus of material

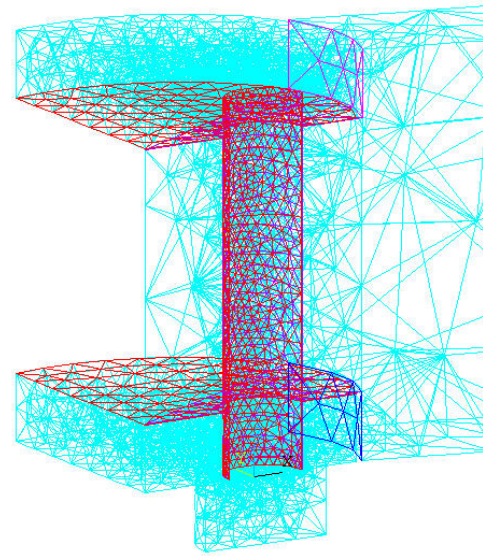


Figure 3.6:
Contact and target elements between bolt and bolt-hole and discs and beam

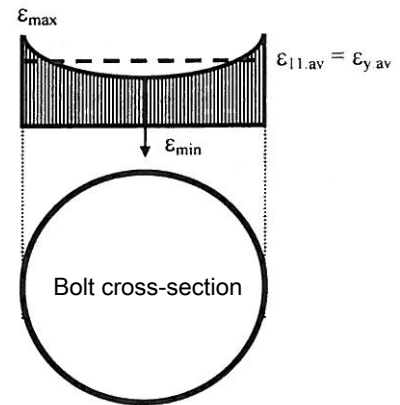
Therefore, in the case of this test for node connector HEFI-1, the optimal contact stiffness is somewhere in the region of $2100 \leq f \leq 2100 \times 10^4 \text{ N/mm}^2$.

For the contact simulating of subjected model HEFI-1, as shown in Figure 3.6, 3-D 8 nodes surface-to-surface contact element CONTA 174, which has three degrees of freedom at each node with translations in the nodal x, y and z directions, with 3-D target surface element TARGE 170 were simulated for the important interfaces between vertical disc plates and beams, horizontal surface of disc plate and end part of beam as well as the surfaces of bolts [ANSYS v.11 2009]. The sticking and sliding conditions are applied with the classic isotropic Coulomb Friction's law [Coelho et al 2006].

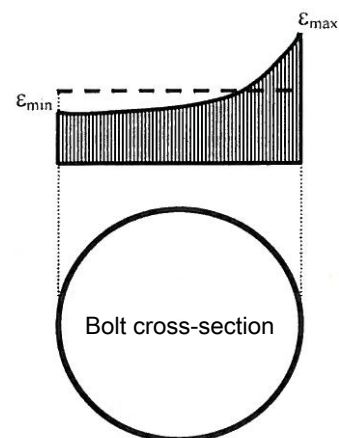
3.1.3 Failure criteria

Due to the other similar literatures based on the steel T-stub connection, the failure criteria should be introduced in this section. The deformation capacity of a connection system is related to the plate or bolt resistance which is determined by bolt fracture or cracking of plate material. In both situations, the modeling of the failure condition can be defined by assuming that cracking occurs when the ultimate strain $\epsilon_{u,b}$ is obtained, either at the bolt or at the plate [Faella et al 2000] [Gioncu et al 2000]. Due to the nature of the materials, the bolt deformation is considerably less than the plate. The ultimate strain of constructional steels is 25-30% at least, while for high strength bolts the ultimate strain is about 5-6% [Swanson 1999]. Consequently, most ultimate conditions are governed by bolt failure and its assessment is of main importance [Coelho et al 2006].

The potential failure mechanisms of a bolt under axial loading are: (a) tension failure, (b) stripping of the bolt threads and (c) stripping of the nut threads. Swanson points out that high-strength fasteners are designed so that tension failure of the bolt occurs before stripping of the threads [Swanson 1999]. The stripping should not be expected in most cases. In addition, such failure ty-



(a) Under pure axial tension



(b) Under combined tension and bending

Figure 3.7:

Layout of the strain distribution in a bolt cross-section [Coelho et al 2006].

pes are not easily opened to a numerical or analytical realization. Hence in many cases, the ultimate deformation of the bolt is governed by tension failure [Coelho et al 2006].

As a structural part of the connection system, the bolt is usually subjected to combined tension and bending. In this case, as shown in Figure 3.7, the strain distribution at the bolt critical section changes from a symmetric distribution to unsymmetrical one. The bolt axis direction is no longer a principal direction. However, if a similar failure criterion is adopted to the single bolt in tension respecting to the maximal average principal strain, i.e. $\epsilon_{11,ave} = \epsilon_{u,b}$ the deformation capacity of the bolt in combined tension and bending can be determined. Thus since the bolt is subjected to combined tension and bending deformations, it has been concluded that failure should be estimated by comparison of the maximal average principal strain ($\epsilon_{11,ave}$) with ultimate strain ($\epsilon_{u,b}$) [Coelho et al 2006].

3.1.4 Material properties

The materials of each beam and the circle discs for the experiment were steel DIN EN 10025 S355JO and E335 respectively. The cylinder-head bolt was based on DIN EN ISO 4762 M12 and the mechanical properties of

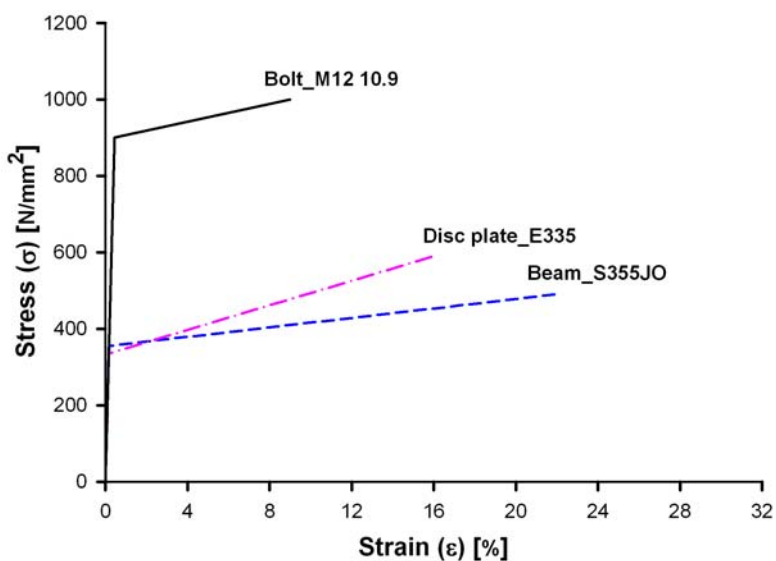


Figure 3.8: Stress-strain curves of bolt, disc and beam element [Fischer 1993]

bolt grade was 10.9.

The E-Module of 210000 N/mm² was applied for all material with a Poisson's ratio of 0.3. In order to simplify for plastic failure criteria, the stress-strain curves for all material was applied as a bilinear (Figure 3.8). For the material nonlinearity, an elastoplastic constitutive regulation with isotropic strain hardening based on the Von Mises yield criterion is adopted.

The condition of contact surfaces were assumed to be cleaned by wire brushing or flame cleaning with any loose rust removed as mentioned in Eurocode 3. Therefore, the coefficient of friction (μ) between the circle discs and beam element and between surfaces of bolt and bolt holes were introduced as 0.3.

3.1.5 Loading and boundary conditions

As shown in Figure 3.9, one-fourth of all geometry of experimental model is symmetry around the central x- and y-axis. However, only two beam members are supported on roller supports, 450 mm distance from the center line of node connector to outer supporting, which would not constrain the horizontal direction. Hence only a half of one beam constrained z-direction was modeled. In order to simulate this supporting condition on the FE analysis, one single vertical roller boundary condition is applied at this point. Two disc plates could be assumed to be at one-fourth symmetrical geometry, because behaviors of two discs are symmetrical of whole discs

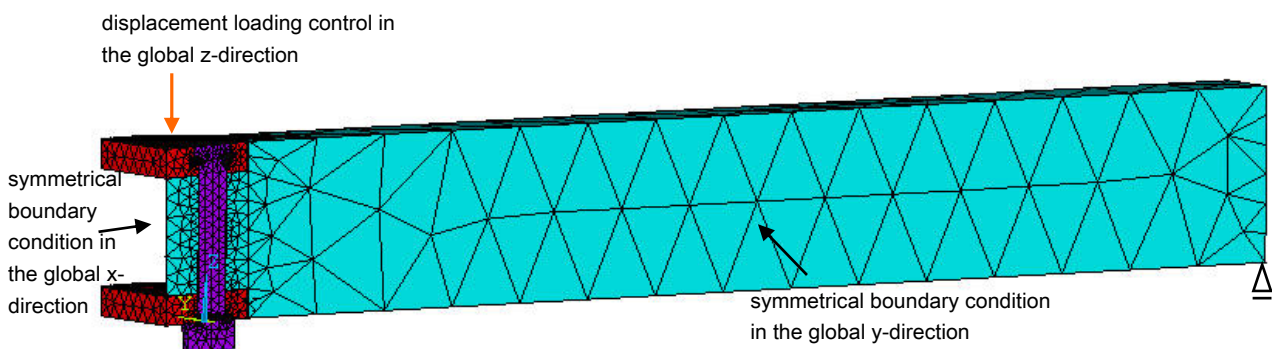


Figure 3.9: Mesh discretisation and FEA boundary conditions with loading

around the central x- and y- axis.

In terms of loading condition, because the model HEFI-1 was not applied prestress, only one load step was used to apply the load. It should be noted that the applied load was controlled by displacement at the top of center on the above disc plate in the negative z-direction to avoid the rigid body motion which may cause convergence difficulties.

3.1.6 Experiment and FEA results

Based on the real experimental results of node connector system HEFI-1, the Finite Element Analysis (FEA) of three points bending test was performed. For real experiment, three tests were carried out and compared with the FEA result.

In case of the experimental results, with the exception of test number 1, the load-displacement curves show an obvious linear elastic behavior until around 50% of failure loads. Subsequently, disproportional progress of plastic behaviors appeared with increased loading in the joint area. The ultimate failure occurred in the two connecting parts that were restrained only by vertical sup-

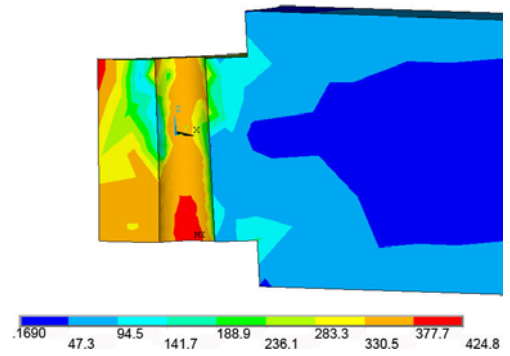


Figure 3.10:
Von Mises stress distribution of the beam

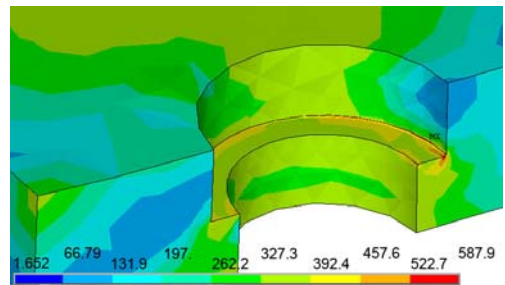


Figure 3.11:
Von Mises stress distribution of the disc plate

```
NODAL SOLUTION
STEP=1
SUB =35
TIME=.955041
SEQV (AVG)
DMX =39.256
SMN =.180498
SMX =998.524
```

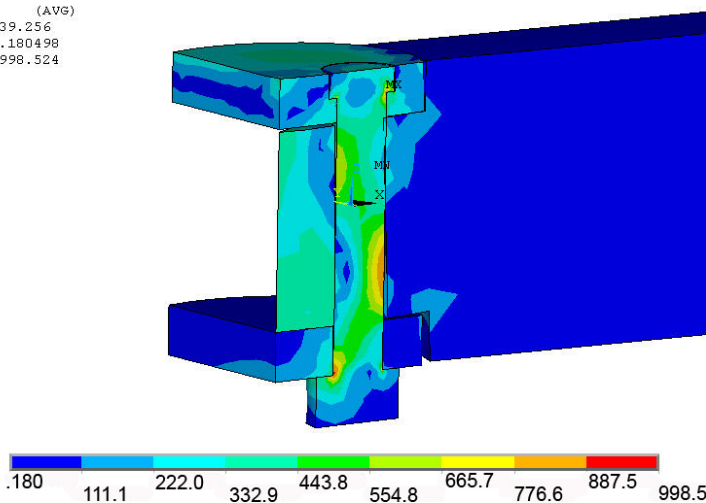


Figure 3.12: Von Mises stress distribution of FEA test and failure mode of specimen

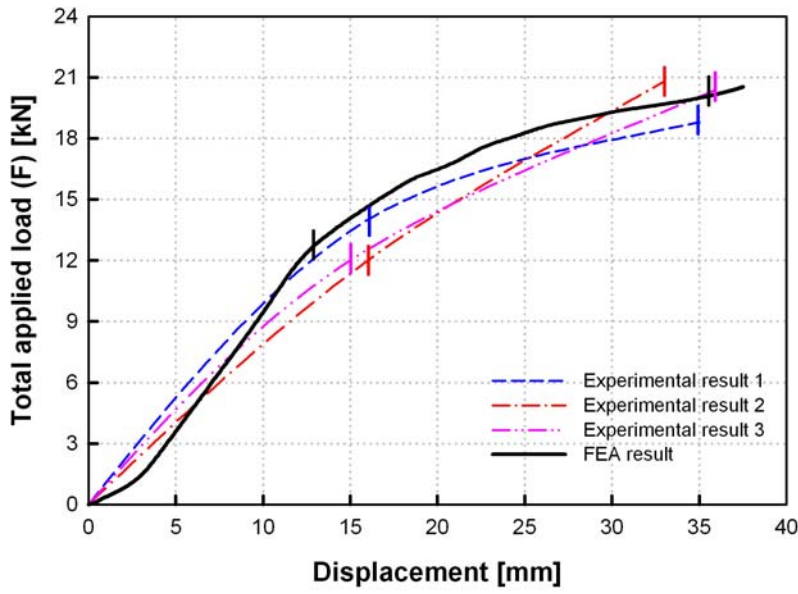


Figure 3.13: Load-displacement curves of experimental and FEA results

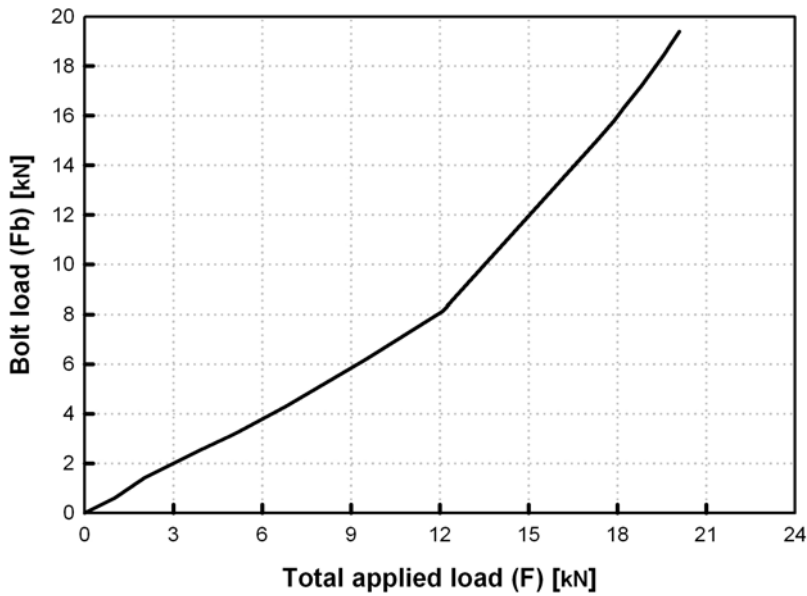


Figure 3.14: Comparing between total applied load and bolt load

Table 3.1: Results of experiment and FEA

	Yield applied load (kN)	Displacement (mm)	Ultimate applied load (kN)	Displacement (mm)
Experiment 1	14.00	16	18.80	35
Experiment 2	12.00	16	20.80	33
Experiment 3	12.00	15	20.40	36
FEA results	12.6	13	20.90	35.5

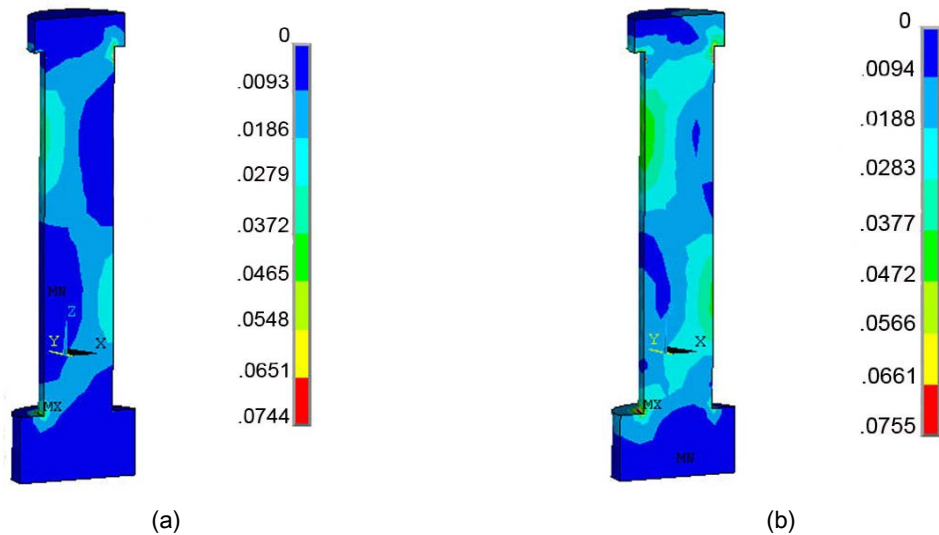


Figure 3.15: Maximum average principle strain ($\epsilon_{11,ave}$) (a) and maximum ultimate strain of bolt ($\epsilon_{u,b}$) (b)

porting, as expected (Figure 3.13).

Figure 3.13 and Table 3.1 show the results of total applied load-displacement curves of experimental and numerical results. The vertical indications on each curve show the yield points and ultimate limits of the material. The overall stiffness of the FE-model is somewhat stiffer than the experiment behaviors because the bolt head and the beam element are assumed to be fully connected to reduce the calculating time as mentioned before. However, the agreement of results are appropriate comparing experimental results 1,2 and 3. For example, the yield load and ultimate applied load of FEA result in 12.6 kN and 20.90 kN, which agrees with experiment 2 at 95 % and 99.5 %, respectively.

In terms of determining failure criteria, for the global deformation of 35.5 mm, the value of maximum average bolt strain ($\epsilon_{11,ave}$) was 7.4 % and the maximum ultimate strain of bolt ($\epsilon_{u,b}$) was 7.5 %. These values are very close to each other, which means both the tension and bending deformations effected the bolt together (Figure 3.15).

Figure 3.12 indicates the Von Mises stress contours at the last step of load before failure. While the maximum stress of bolt reached up an ultimate limit of around 1000 N/mm², the material strength of the beam and disc plate

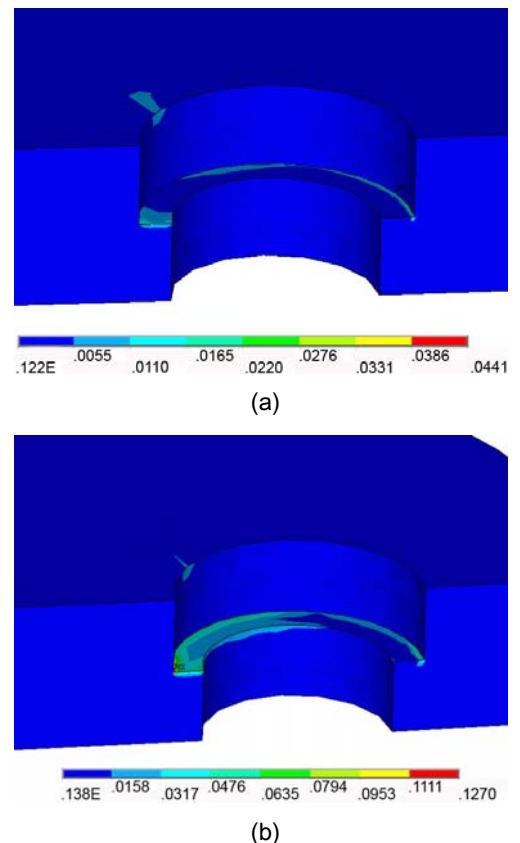


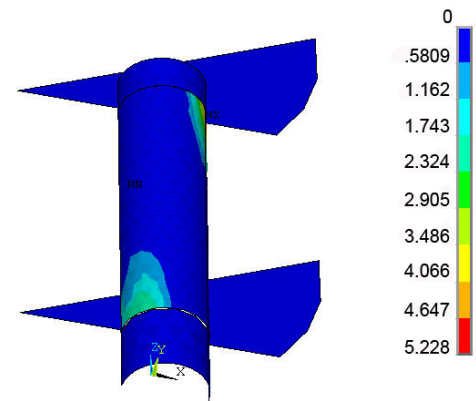
Figure 3.16: 1st plastic principal strain ϵ_{11} in the disc plate at the applied load level 12.6 kN (a) and 20.9 kN (b)

were 423 N/mm² and 587 N/mm², respectively, which means that the material capacity of beam and disc plate almost arrived at the ultimate state (Figure 3.10 and 3.11).

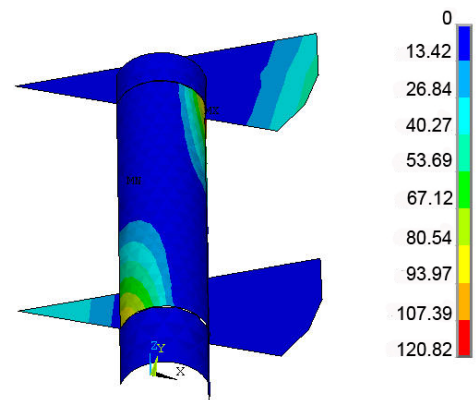
The evaluation of the real load in the bolt should be known because it can influence the resistance of the connector and especially, the failure mode. Figure 3.14 shows the development of bolt load (F_b) with the total applied load (F). The measured force in the bolt was obtained from the product of the recorded strain, E-module of the bolt and the shank area. In order to find out the influence of disc plate on the bolt, the bolt force computed by FEA was calculated by the bolt area with the stress at the bolt mid-plane, allowing a uniform distribution of force for all bolts. It shows that the yielding of disc plate begins at a total applied load level $F=12.6$ kN and it increases up to 19.4 kN.

As shown in Figure 3.16, the plastic strain of disc plate occurred on the surface of upper bolt hole and was 4.44 % at the total applied load level 12.6 kN, which means that the plastic behavior in the disc plate has already started. And when the bolt faced the ultimate failure load level, the plastic strain of beam was almost 13 % which can be easily assumed to be beginning signs of disc plate failure. From this interaction of load in the connector, the main failure mode is the combination of bolt's and disc plate's deformation.

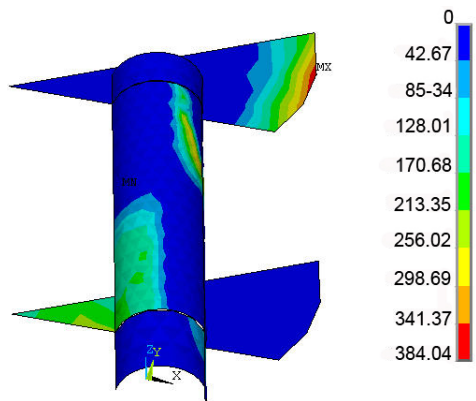
This phenomenon can be also seen in the development of contact surface pressure. As shown in Figure 3.17, when the total load started on the node, the contact pressure was only on the surface of the bolt. However, from the load level (F) 12.6 kN, the significant prying force between disc plates and end beam was introduced with the shear force of the bolt. As a result, the stress of contact pressure between disc plates and end beam became higher than at the failure load level 20.9 kN, and then followed by the total failure of connecting system. Thus, it can be clearly seen that the disc plate plays a very important roll for the transfer of force in this connecting system, so that the structural capacity of the connector could be increased.



(a) $F=0.106$ kN, $\delta=0.4$ mm



(b) $F=12.6$ kN, $\delta=11$ mm



(c) $F=20.9$ kN, $\delta=35.5$ mm

Figure 3.17: Progress of contact stress with applied load (bolt clearance 0.1mm)

3.2 Node connection system SBP-3

To design the inner court roof of the DZ-Bank in Berlin, as shown in Figure 3.19, Schlaich Bergermann & Partner developed the splice connection system SBP-3 (Figure 3.18). The node connector consists of a solid plate with 6 horizontal finger splice plates. The end of the beam member was fabricated as a fork-shaped fitting, which the 6 horizontal finger splice plates can be inserted and connected by two or more bolts in double shear surfaces. The important accommodation of horizontal, vertical and twist angles of the structural member at this node connection was dependent on the machining of the finger splice plates.

3.2.1 Geometrical details of experiment

This node connector consists of a solid plate as node with 6 horizontal finger splice plates. The end of the beam member was fabricated with fork-form fittings, which can be connected to the connector fabricated with finger splice plates of the node by two or more countersunk bolts (M12) in double shear without preload. The length of each beam including center of node is 1300 mm. The cross section of member for the experiment is 40 mm × 60 mm. As shown in Figure 3.22, the total length of node is 300 mm with 100 diameter of center part of node and the horizontal angle of each beam is 60°.

Contrary to the 3-points bending test for HEFI-1, the beam member was constrained on each of the roller supportings. In terms of bolt clearance between bolt-hole and bolt, the deviation was fabricated at 0.1 mm.

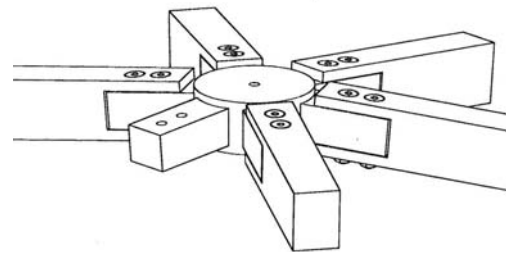


Figure 3.18:
Node connection system SBP-3
[Stephan et al 2004]



Figure 3.19:
View of roof in DZ Bank, Berlin
[Schlaich et al 2003]

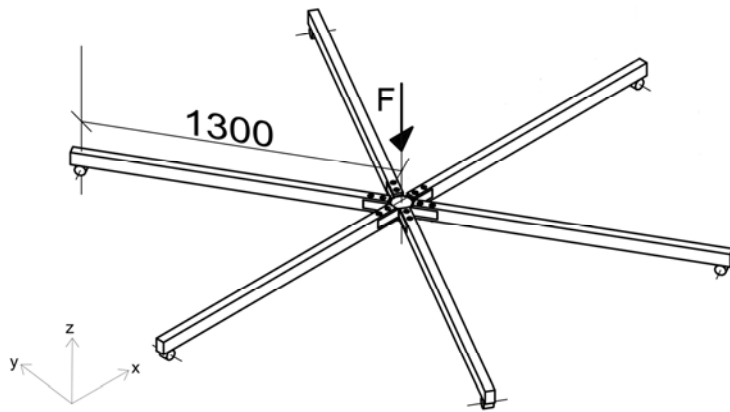


Figure 3.20: Test set-up of bending test (mm)



Figure 3.21:
Experimental setup of bending test with
node connection SBP-3

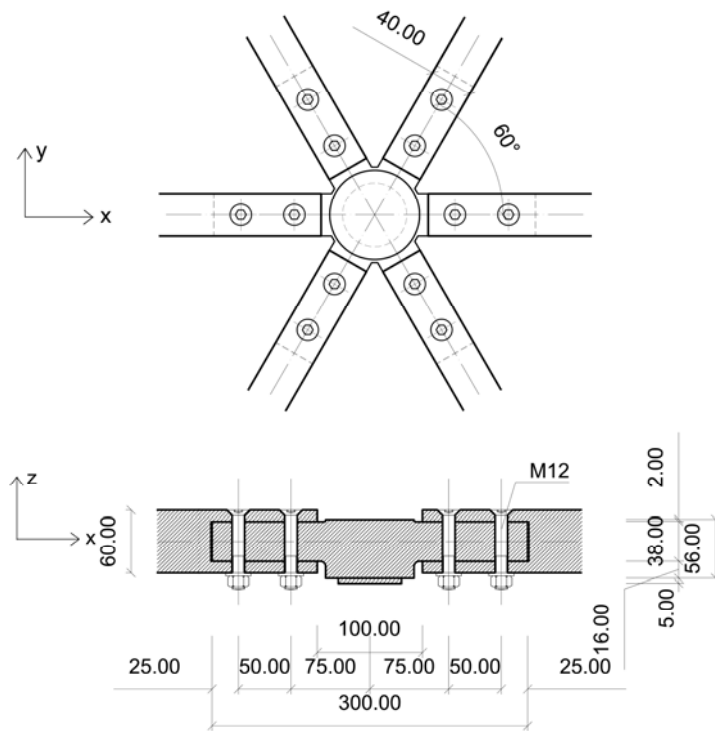


Figure 3.22: Details of SBP-3 (mm) [Schlaich et al 2003]



3.2.2 Finite element model

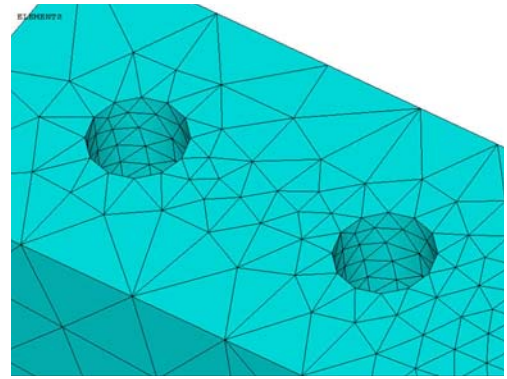
For simulation, most of the FE modeling, in this FE analysis, could be implemented as the modeling of HEFI-1, because the previous FEA of HEFI-1 was successful.

Based on the function of ANSYS, node, beam member and bolt could be meshed by the 10-node tetrahedral solid structural element SOLID 92. Due to the 3 dimensional CAD program Rhino version 4.0, all geo-

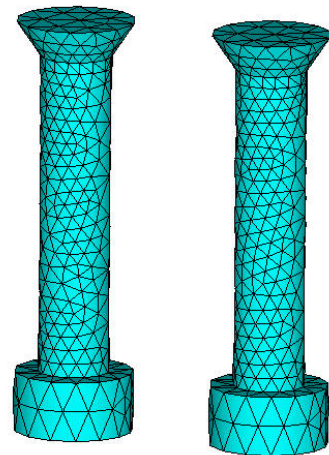
metry could be modeled for analysis. To reduce the number of contact planes, the bolt head and nut are assumed to be fully connected. This simplification may lead to somewhat stiffer deformation, however the overall behaviour is not greatly influenced, as already mentioned in the references [Coelho et al 2006].

Figure 3.24 shows the FE mesh that was simulated for the analysis. As in the other finite element analysis, a refined mesh is always very important. However, if the simulation geometry is large-scale, the calculating time should be also considered. Thus a proper discretization, in which main stress will occur, should be designed as well.

In this case, especially, the bolt discretization requires a reasonable mesh, because the complex state of stress appears on the bolt. The number of elements is determined decisively by the discretization of the circumference of the bolt. Other researches and literatures have suggested a minimum of 12-16 nodes around the circular hole [Virdi 1999] [Coelho et al 2006].



(a)



(b)

Figure 3.23:
The finite element mesh of splice plate of node (a) and bolts (b)

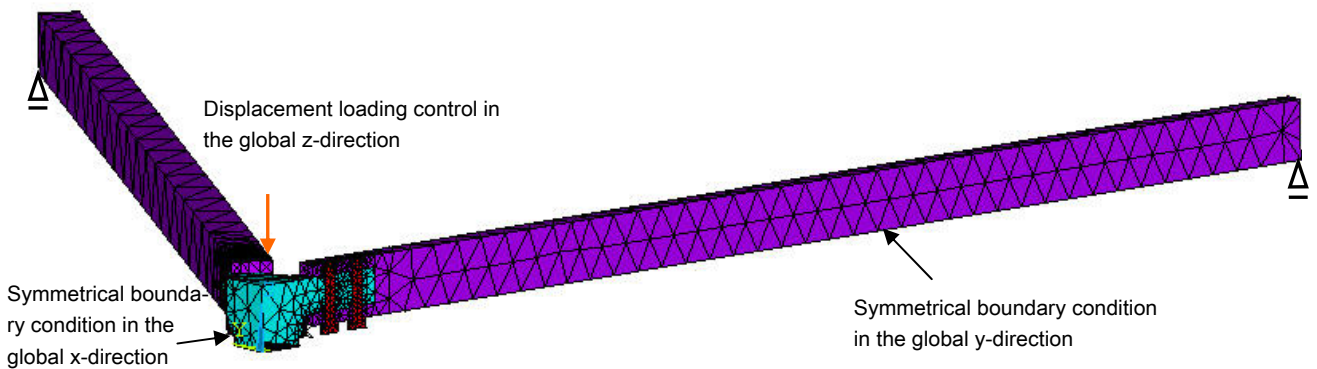


Figure 3.24: Mesh discretization and FEA boundary conditions with loading

Based on the above conditions, the author used a function of ANSYS, namely smart meshing design tool. As a result, a very reasonable mesh could be obtained, taking into particular consideration not only for a refined mesh but also for a calculating time so that the successful convergence could be brought into the results (Figure 3.23).

Regarding contact element, 3-dimensional 8 node surface-to-surface contact element CONTA 174 with 3 dimensional target surface element TARGE 170 were matched for the important interfaces between end of beam member and finger splice plate of node. Also, the surfaces of bolt-holes were also simulated by contact and target elements [ANSYS v.11 2009].

3.2.3 Material properties

Based on the experimental data, three different material properties were adopted respectively. The node material was stainless steel 1.4301-S355 and for the numerical simulation, the available yield strength of 355 N/mm² was used. For the beam element, stainless steel 1.4301-S235 was used and the yield strength for the calculation was 190 N/mm². According to DIN EN 10088-1, E-Module of 200000 N/mm² was applied for all material with a Poisson's ratio of 0.3. The stainless bolts A4-70 were used.

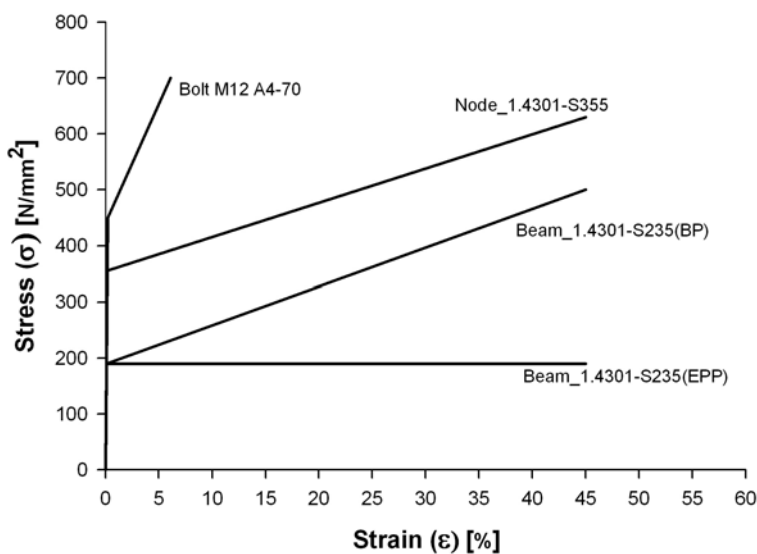


Figure 3.25: Stress-strain curves of bolt, disc and beam element of SBP-3

To calibrate the results obtained from the numerical model, two different types of stress-strain curves for the beams were introduced. At first, the elastic-perfectly plastic (EPP) behavior was applied, and secondly, the stress-strain relationship was taken as a bilinear (BP).

The elastic and ultimate limit of bolts were defined by DIN EN ISO 3506-1, and the plastic strain of bolts was able to be adopted by Ramberg-Osgood's relation which was introduced in other similar literature [Bouchaír et al 2008].

$$\varepsilon = \frac{\sigma}{E_0} + 0.002 \times \left(\frac{\sigma}{\sigma_{0.2}} \right)^n \quad (3.3)$$

ε : the strain

$\sigma_{0.2}$: the 0.2% proof stress (elastic yield), σ : the stress

E_0 : Elastic modulus

n : a coefficient of the material strain hardening

This relation is often used by EN-1993-1-4 to represent the non-linear behavior of stainless steel. It could be improved for the part above the elastic limit [Rasmussen 2003]. However, if the n parameter is well chosen the relation can describe accurately the stress-strain relationship. Actually, the n value should be experimentally obtained by coupon test. However, due to the similar literature, the coefficient of n could be taken as 7.6 for the simulation [Bouchaír et al 2008]. Other properties of the stainless steel bolt A4-70, which was used for experiment given by DIN EN ISO 3506-1, are as follows, the 0.2% proof stress $\sigma_{0.2}$ was 450 N/mm² and the ultimate stress σ was 700 N/mm².

In case of the stress-strain curves of beam and node element, the elastic-perfectly plastic (EPP) behavior was taken to simplify the calculating procedures and time. The stress-strain curves used in this numerical model are given in Figure 3.25. The coefficient of friction (μ) for the contact surface between node and beam was taken as 0.3.

3.2.4 Loading and boundary conditions

Due to their geometrical symmetry about the central axis, an one-fourth symmetrical model is used to save computation time (Figure 3.24). As shown in Figure 3.20, the force was loaded at the middle of the node and the boundary conditions of the roller were positioned at a distance of 1,300 mm from center of the node.

Three displacement transducers were installed to estimate node displacement and beam displacement as well. As shown in Figure 3.27 while two displacement transducers were calculated by two beams, one displacement transducer was estimated under the node. To obtain a global load-displacement curve, the transducer under the node was adopted here as shown in Figure 3.28.

In order to observe only the node connector's stiffness without member stress as much as possible, all the boundary conditions at the end of the member were only vertically restrained by roller, which means that the horizontal supporting in each local direction is totally free.



Figure 3.26:
Strain gauge under the node connectoin



Figure 3.27:
View of loading on the center of node and two strain gauges

3.2.5 FEA and experimental results

With the mentioned above numerical conditions mainly based on experimental information, the finite element analysis for node connection system SBP-3 were carried out.

The results of this simulation are based mainly on the global load-displacement curves. Figure 3.28 shows the total applied load-displacement curves of the experiment and FEA using two different material characteristics for the beam material.

As shown in Figure 3.25, elastic-perfectly plastic (EPP) and bilinear plastic (BP) were adopted for the end of the beam members. As usual, for a simplified approach to steel structure, the elastic-perfectly plastic law could have been applied. However, because stainless steel has strong strain hardening characteristics, more detailed definition of plastic material behavior was needed for the analysis [Bouchaír et al 2008]. Moreover, these two different plastic behaviors of material were required to calibrate the FEA results with experimental result.

Figure 3.28 presents that the initial stage of loading for EPP and BP are linear and that the agreement between all FEA curves and the experimental result are very close.

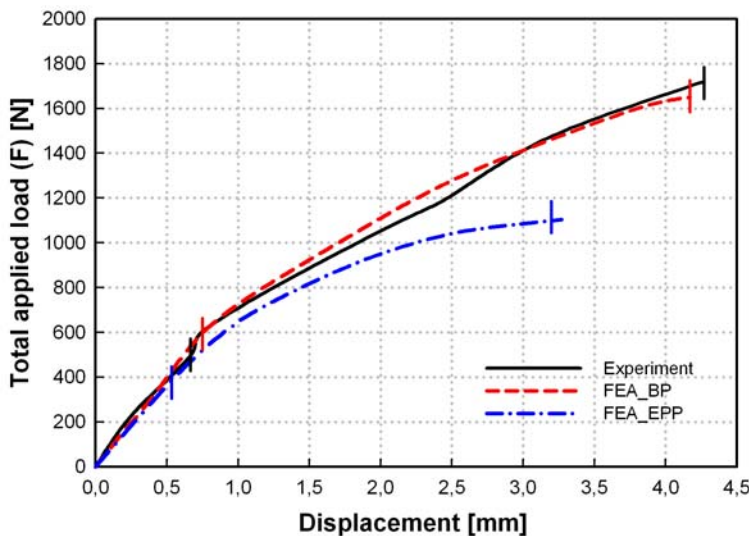
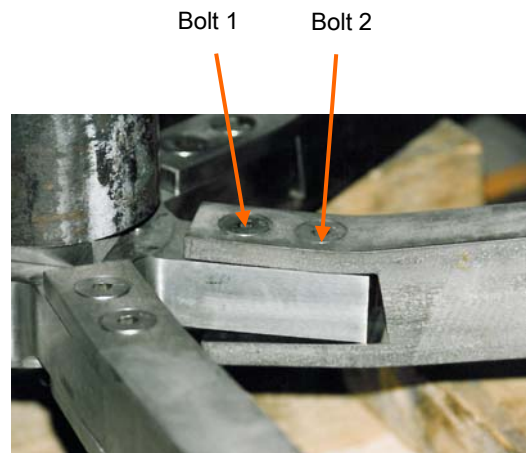
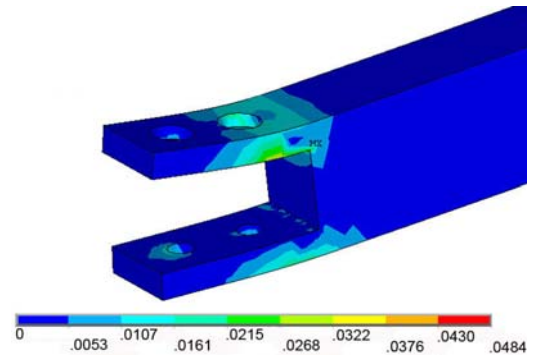


Figure 3.28: Load-displacement curves of experimental and FEA results for SBP-3



(a)



(b)

Figure 3.29: Plastic deformation of end beam (a) and 1st plastic principal strain ϵ_{11} of FEA in the beam (b) at the total load level 1670 N (superelevation 10 times)

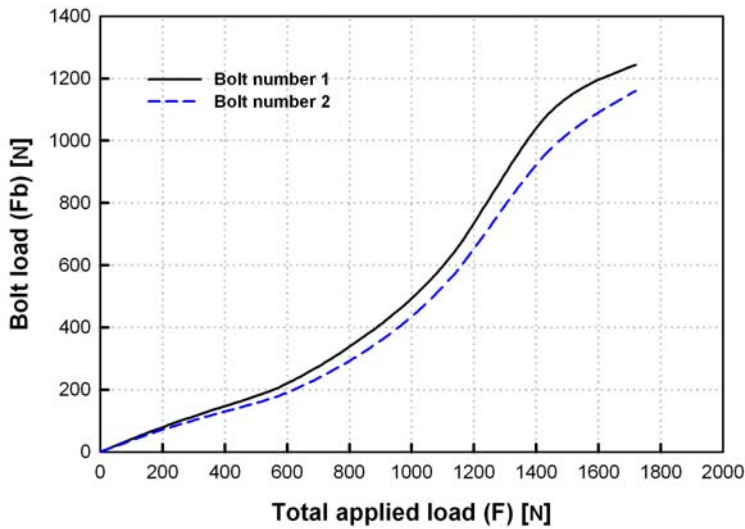


Figure 3.30:
Comparing between total applied load and bolt loads

The difference between the EPP and BP, however, starts with the development of plasticity. The load-displacement curve of EPP shows a lower stiffness than BP's curve, because EPP behavior already reached the plastic plateau while strain hardening of BP continued.

The failure mode corresponds to the appearance of plastic hinge in the end of beam caused by bending and then to the failure of the bolts subjected to combined tension and shear stresses. While the bolts were loaded to the ultimate stress of around 700 N/mm^2 , the first plastic principal strain was about 5 %, which means the plastic hinge had already appeared (Figure 3.29). Consequently, as shown in Figure 3.28, the numerical result,



(a)

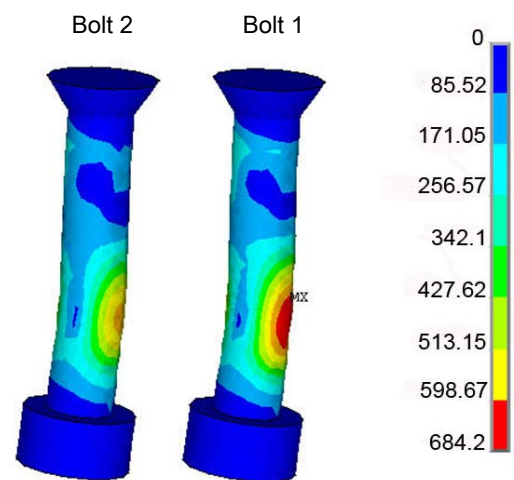


Figure 3.31:
Bolt failure of experiment (a) and maximum von Mises stress in the bolt from FEA (b) (superelevation 10 times)

Table 3.2: Yield and ultimate applied loads of experimental and FEA

	Yield applied load (N)	Displacement (mm)	Ultimate applied load (N)	Displacement (mm)
Experiment	500	0.67	1720	4.27
FEA_BP	530	0.70	1670	4.17
FEA_EPP	480	0.63	1103.8	3.27

in the case of BP, shows a very reliable failure mode in the real experiment.

As shown in Figure 3.30, the curves representing the total applied load, versus the bolt's load progress, show that the load in the bolt is somewhat limited by the deformation at the end of the beam. Nevertheless, when the load continue to apply to the node the last failure mode can be easily expected from the contact interaction in the joints. Figure 3.32 shows the evolution of the stress of contact pressure with the incremented load on the node, which the leverage force introduced on the surface between the end of beam and node. A higher tension and bending force was reveled to be transferred to bolt number one, rather than to bolt number two.

As for the failure mode of the whole node connection, although the plastic hinge appeared early in the end of the beam, the compressive and tensile force could be transferred on the top and bottom area in the fork-shaped beam, so, the total applied load could be beared by the bolts. As a result, this mechanism of loading transfer keeps the whole stiffness of the node connection system SBP-3. Consequently, bolt failure did occurred, and this loading mechanism from this simulation is very compatible with experimental failure mode as shown in Figure 3.29 and 3.31.

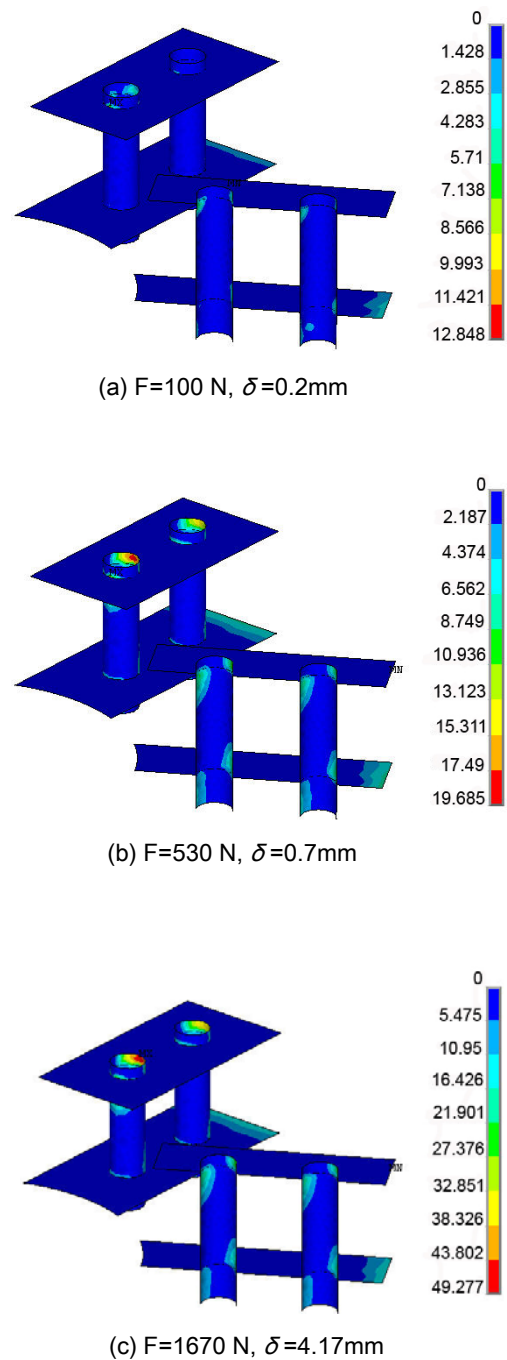


Figure 3.32:
Progress of contact stress with applied load level (bolt clearance 0.1mm)